Journal of Alloys and Compounds 509 (2011) 7466–7472

Contents lists available at ScienceDirect

Journal of Alloys and Compounds

journal homepage: www.elsevier.com/locate/jallcom

Effect of microstructural feature on the tensile properties and vibration fracture resistance of friction stirred 5083 Alloy

Kuo-Tsung Huang, Truan-Sheng Lui*, Li-Hui Chen

Department of Materials Science and Engineering, National Cheng Kung University, Tainan, Taiwan 701, ROC

ARTICLE INFO

Article history:
Received 19 September 2008
Received in revised form 13 April 2011
Accepted 15 April 2011
Available online 23 April 2011

Keywords:
5083 alloy
Friction stirring
D–N curve
Crack propagation

ABSTRACT

In this study, 5083 Al–Mg plates were friction stirred at optimal rotation speeds to investigate the tensile properties and vibration fracture resistance. As a result, grain refinement could be observed at the stir zone with 7 μm average grain size and fine particles could be observed as well. The tensile strain–elongation curves reveal that the tensile strength and elongation tended to increase as the microstructure was refined in the friction stirred sample. The D–N curves of the specimens recorded under an identical initial deflection show that there was a slight difference between the parent metal and the friction stirred sample. A refined grain size is partially responsible for an improvement in vibration fracture resistance; however there is another factor which plays a role too. It should be noted that the deterioration of vibration fracture resistance is a consequence of fine particles stirred into a softened matrix. From the crack propagation results, an intergranular crack propagation feature can be recognized in the friction stirred specimen, and it is reasonable to suggest that the fine particles played an important role in the deterioration of the vibration fracture resistance.

1. Introduction

The need to reduce the weight of components has led to an increase in the use of lightweight materials such as aluminum alloys. The 5083 aluminum solid-strength alloy which has excellent formability, good strength and high corrosion resistance is widely used in the automotive and shipbuilding industries. Moreover, the steel wheels in large vehicles are gradually being replaced by aluminum wheels for the sake of reducing the weight of the car. The aluminum wheels in large vehicles not only have to undergo a joining process but are also subjected to repeated cyclic loading from rough roads. When aluminum wheels perform under adverse circumstances, vibration cracks often initiate at the stress concentration or the lower strength area on the surface and grow into the body of the wheel. The 5083 alloy practically implemented in aluminum wheels shows a tendency towards abnormal vibration (a common cause of failure in aluminum wheels). Severe fracture problems occur especially when the applied vibration frequency meets the resonance [1]. Consequently, the resonant vibration fracture behavior needs to be thoroughly explored.

Meanwhile, the traditional joining process is not suitable for aluminum alloys because of the higher electrical and thermal conductivities. These will lead to higher energy consumption. Friction stir welding (FSW) is a solid-state joining process. Because the melting point of the alloys will not be reached during the joining process, there is no porosity and shrinkage that usually accompanies fusion welds. Thus it is especially suitable for welding aluminum alloys [2]. Friction stir processing (FSP) is a derivative process of friction stir welding. Stir zones in which FSW/FSP are performed can acquire the advantage of grain refinement [3,4]. According to many previous reports [3–5], the friction stir zone possesses fine recrystallized grains resulting from severe plastic deformation. 5xxx aluminum alloys have great potential for refining the microstructure through a deformation process and the mechanical properties of Al–Mg alloys can be enhanced [6,7]. This study focuses on the formation of fine grains through dynamic recrystallization in the stir zone and will furthermore clarify the effect of microstructural evolution on vibration fracture behavior. 5083 Al–Mg alloy was chosen to explore the damping capacity and the vibration fracture behavior under resonant vibration.

2. Experimental procedures

5083 Al–Mg plates were heated at 625 K for 2 h to achieve a fully annealed microstructure, and then the fully annealed plates were given a single pass of FSP as shown in Fig. 1 (tool rotation speeds were 2300 min^{-1}; tool moving speeds were fixed at 160 mm min^{-1} with 1.5° of tool angle; the downward push force was controlled at 19.6 MPa). The chemical composition of the 5083 plate is listed in Table 1. In this study, the parent metal and friction stirred 5083 alloy specimens are designated as 5083 and 5083-FSP respectively.

* Corresponding author.
E-mail addresses: morganhuang@pchome.com.tw (K.-T. Huang), z7408020@email.ncku.edu.tw (T.-S. Lui).

0925-8388/$ – see front matter © 2011 Elsevier B.V. All rights reserved.
doi:10.1016/j.jallcom.2011.04.080

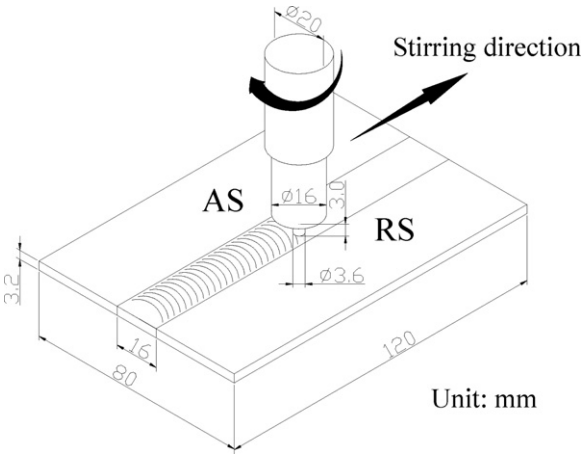

Fig. 1. Schematic illustration of the friction stir process (FSP).

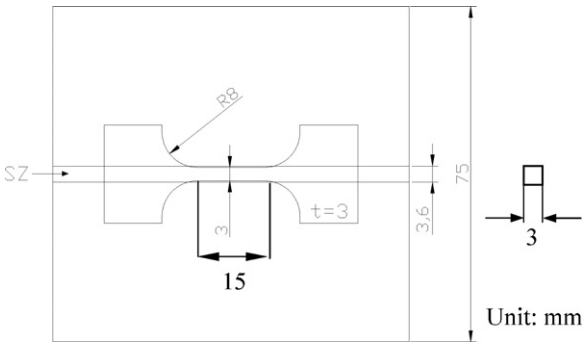

Fig. 2. Schematic illustration of the tensile specimen (FSP).

Table 1
Chemical composition of the 5083 alloy used in this study.

	Mg	Fe	Cr	Si	Mn	Al
5083	4.31	0.18	0.1	0.07	0.89	Bal

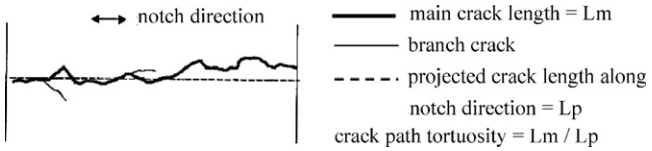

Fig. 4. Schematic drawing of the cracking features generated by resonant.

The microstructural features of the specimens were examined by optical microscopy (OM) and transmission electron microscopy (TEM). thin-foil disk specimens of HF2000 FE-TEM were cut 3 mm in diameter from the stir zone and were then jet electropolished by an electrical discharge machine in a 50 ml HNO_3 + 200 ml CH_3OH solution at 248 K. To study the Vickers hardness profile in the vicinity of the stir zone, the Vickers indenter was set to a 0.98 Nf load for 15 s. In the tensile test, in order to examine the effects of the microstructural features and tensile properties, the strain rate was fixed at $8.3 \times 10^{-4}\ s^{-1}$, and a tensile specimen with 15 mm gauge in length and 3 mm in thickness was used. As indicated in Fig. 2, the FSP specimens were longitudinal to the stir zone.

The vibration specimen and its dimension are illustrated in Fig. 3(a). To generate the vibration, one end of the test specimen was clamped on a vibration shaker. The two V notches adjacent to the clamp were designed to confine the resonance at the stir zone and restrict crack initiation from the notch fronts. In this study, two kinds of vibration test were performed. First, acceleration of the vibration shaker was fixed at 1.1G (17.8 m/s^2). Second, the initial deflection was adjusted to 6.5 mm. Deflection of the specimen at the other end opposite to the vibration shaker was measured by a deflection sensor. As shown in Fig. 3(b), in order to determine the resonance frequency which led to the largest deflection, the vibration frequency was varied continuously. For both the 5083 and 5083-FSP specimens, the resonant frequencies were in the range of 41 ± 1 Hz. Fig. 3(c) schematically depicts the vibration setup.

The microstructural differences of the specimens on the crack propagation paths were examined by an optical microscope equipped with an image analyzer. All specimens were surface finished by polishing with 0.3 μm Al_2O_3, so the cracking path through the microstructure could be directly observed. Consequently, quantitative data of crack tortuosity could be determined by the method shown in Fig. 4. The crack tortuosity value can be defined as the main crack length divided by the projected crack length along the notch direction (shown by the broken line in Fig. 4). The projected crack length is parallel to the tip direction of the two V-notches (i.e., the notch on the stir zone, as indicated in Fig. 4).

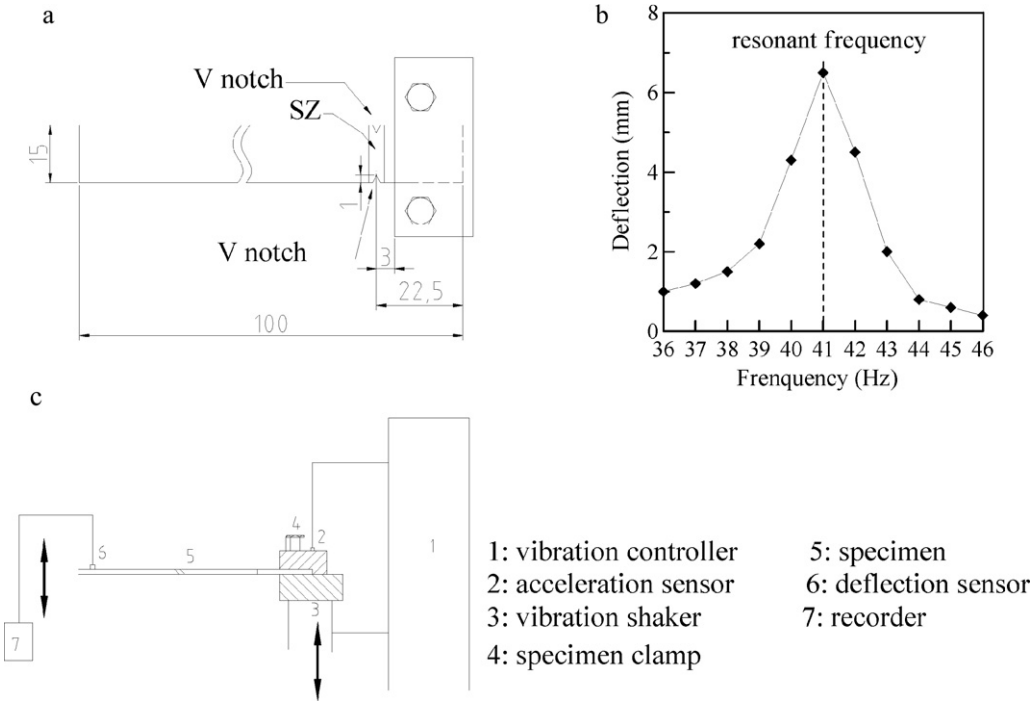

Fig. 3. Shape and dimension of the resonant vibration test specimen for (a) vibration geometry and dimension, (b) resonant frequency, and (c) the resonant vibration setup.

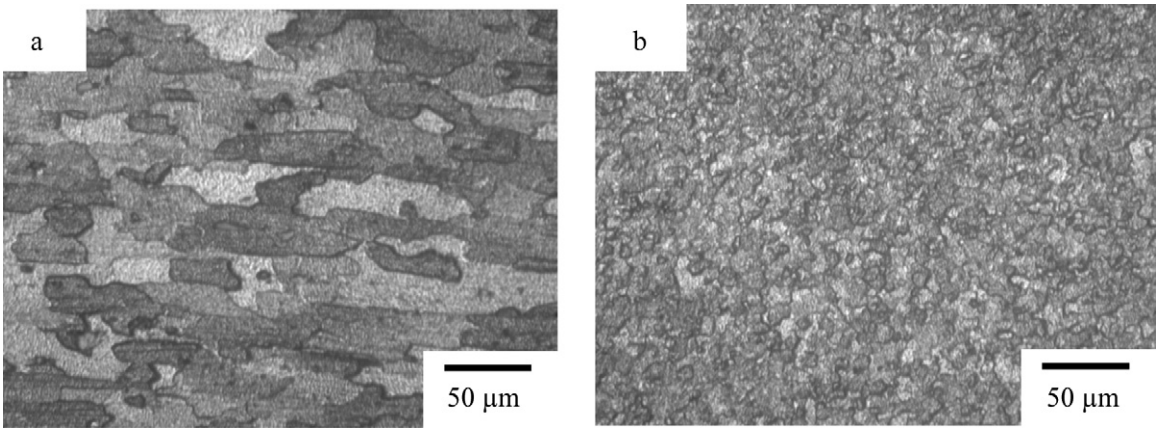

Fig. 5. Optical Microscopic of (a) 5083, and (b) 5083-FSP.

Table 2
Tensile properties, average grain size and *n* value of the 5083 alloy.

Specimen	U.T.S. (MPa)	Y.S. (MPa)	U.E. (%)	T.E. (%)	*d* (μm)	*n*
5083-FSP	332.4	175.7	20.3	25.9	7	0.27
5083	319.5	142.3	16.0	22.7	30	0.34

3. Results

3.1. Microstructural feature and tensile properties

Fig. 5(a) shows that the 5083 specimen has a typical metallography. As indicated in Fig. 5(b), the 5083-FSP has a fine equiaxed grain structure in the stir zone. In terms of the average grain size, there is a significant difference between the microstructure of the 5083 and 5083-FSP samples, as shown in Table 2. Though the 5083 sample was given a full annealing treatment, its aspect ratio through the cross section is 1.9:1. The TEM images of the specimens are shown in Fig. 6. The 5083 specimen, exhibiting coarse grains with a low density of dislocation and a high density of fine particles, is shown in Fig. 6(a). Fig. 6(b) shows that 5083-FSP had fine equiaxed grains and sub-boundaries with a low density of dislocation and a high density of fine particles. Meanwhile, finer particles are observed in the vicinity of the equiaxed grains in the 5083-FSP as shown in Fig. 6(b), whereas the particles in the 5083 specimens are shown in Fig. 6(a).

In addition, microstructural imhomogeneity of the 5083-FSP specimen can be observed from the microhardness profiles along the cross section of the stirred specimen, however, from the base metal to friction stirred zone, the microhardness profiles show a slight difference as represented in Fig. 7. Nevertheless, it should be noted that even slight variations in microhardness can cause significant changes in fracture resistance. Consequently, in the following tensile test, in order to eliminate the influence of advancing or retreating microstructure, specimens were cut entirely from the stir zone. Fig. 8 shows the stress–elongation curves, both the 5083 and 5083-FSP specimens have a serrated yielding behavior. It is clear that the friction stirred specimens displayed an improvement in deformation resistance, and this can be easily proven by comparing the results shown in Fig. 5 which clearly show that grain refinement is very effective in enhancing tensile properties.

3.2. Vibration fracture resistance and crack propagation features

Fig. 9 shows the vibration test results presented in the form of D–N curves (deflection amplitude vs. number of vibration cycles). The D–N curves suggest that the deflection amplitude can be classified into three stages. As illustrated in Fig. 9(b), both the 5083 and

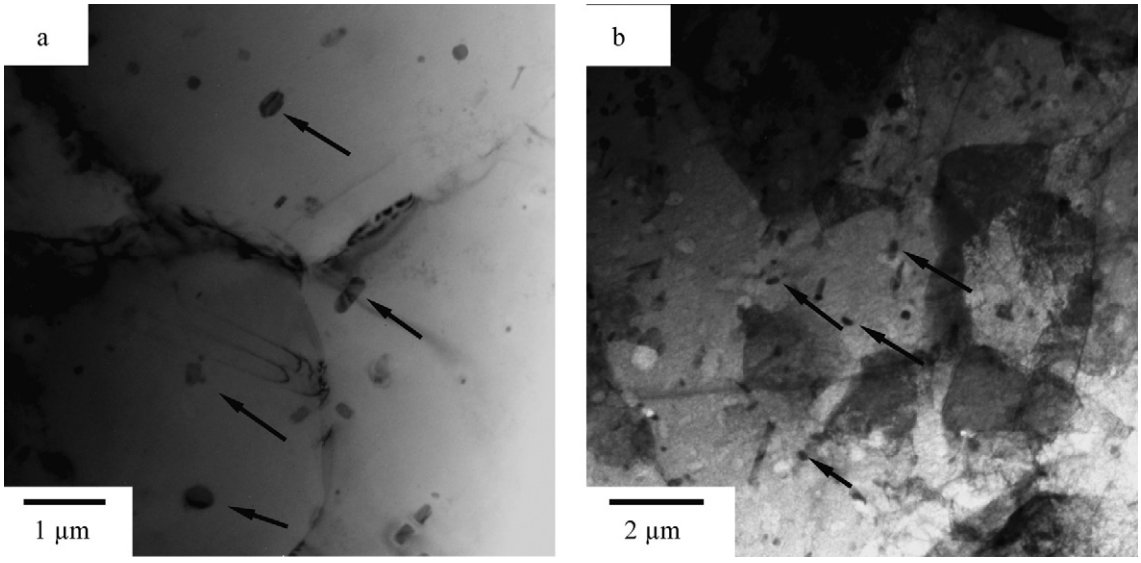

Fig. 6. TEM micrographs of (a) 5083, and (b) 5083-FSP.

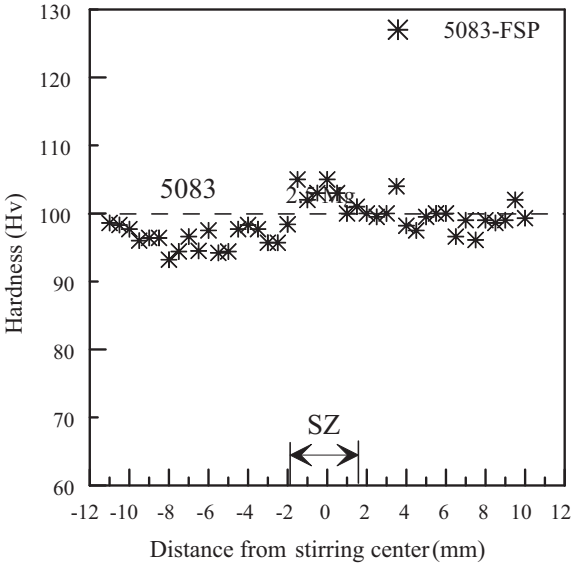

Fig. 7. Hardness profile across the stir zone.

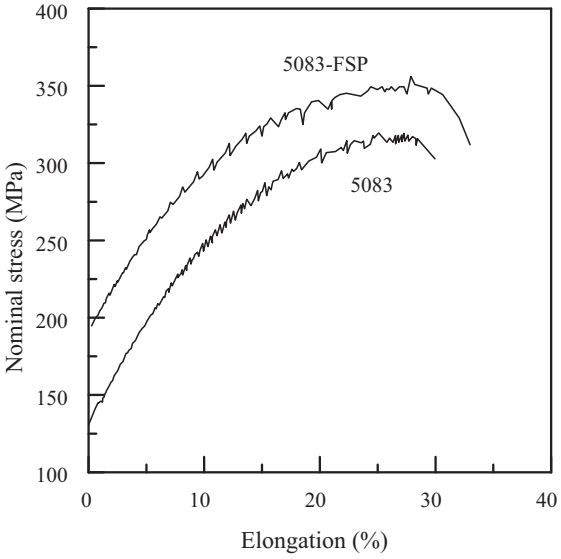

Fig. 8. Relation between stress and elongation.

5083-FSP specimens exhibit the same trend of increasing deflection in the initial stage and decreasing deflection in the final stage. The figure also shows a distinct plateau stage of maximum deflection in-between the initial ascending stage and the final descending stage. Sometimes the D–N curves do not possess a distinct plateau stage as shown in Fig. 9(a).

Fig. 9(a) shows that the D–N curves of both test specimens were recorded under an identical acceleration (1.1G). The 5083 and 5083-FSP samples had no distinct difference in their D–N curves. This is probably related to the stirring area which occupied only a small area of the vibration sample. To avoid the effect of damping capacity, in this study, the vibration force of the specimens was controlled to obtain identical initial deflection amplitudes. This allowed us to measure the vibration cycle of the D–N curves under constant vibration strain conditions (i.e., identical initial deflection conditions). Under the initial deflection of 6.5 mm, the D–N curves of the friction stirred samples are only slightly better than the base metal. These results can be further compared with their *n* values as shown in Table 2. The slope of ascending deflection amplitude of the 5083 specimen which has larger *n* values is also steeper. Consequently, the 5083 specimen has better work hardening behavior. This can be attributed to its microstructural characteristics resulting from the annealing treatment which lowered the vibration fracture resistance.

Furthermore, the vibration fracture features can also be examined by observing the fracture surfaces. Fig. 10 reveals a significant difference in the 5083-FSP and 5083 specimens. Fig. 10(b) shows the 5083-FSP specimen with a faceted fracture pattern which resulted from its fine equiaxed grain structure. The 5083 specimen has a typical feature in the propagation regime. The vibration fracture surfaces reveal signs of ductile fracturing which gave rise to rugged crystal planes as shown in Fig. 10(a). As for the vibration fracture resistance, the crack propagation behavior will be influenced by microstructural variations. Fig. 11 reveals that there is a significant difference in the crack propagation behavior of the 5083 and 5083-FSP specimens. The 5083 specimen shows a few slip bands in the vicinity of the main crack when the deflection amplitude reached the maximum, which is shown in Fig. 11(a).

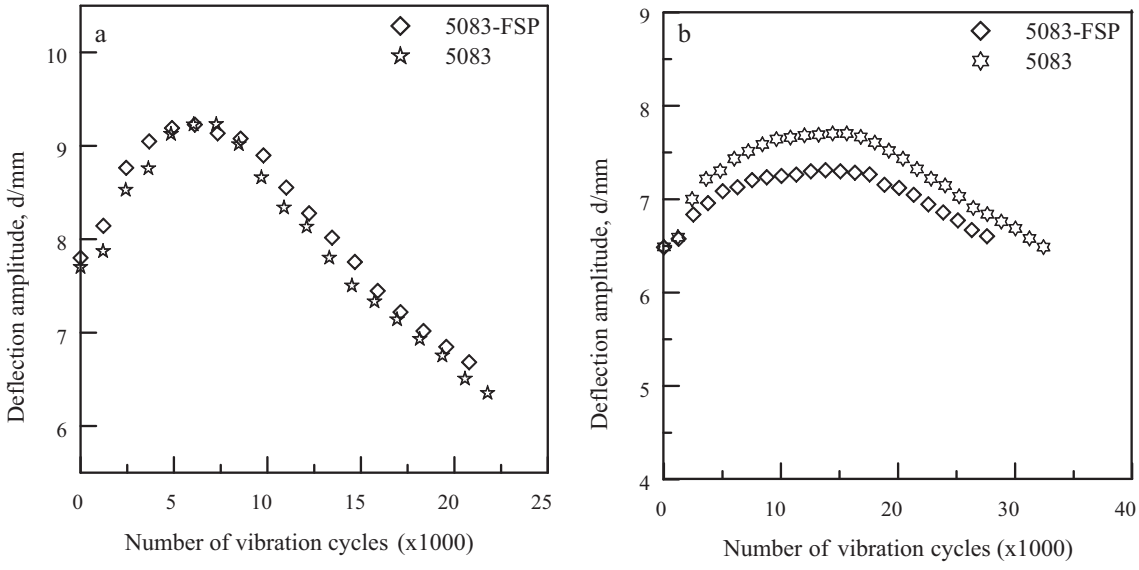

Fig. 9. Deflection vs. number of vibration cycles curve (a) 1.1G, and (b) D = 6.5 mm.

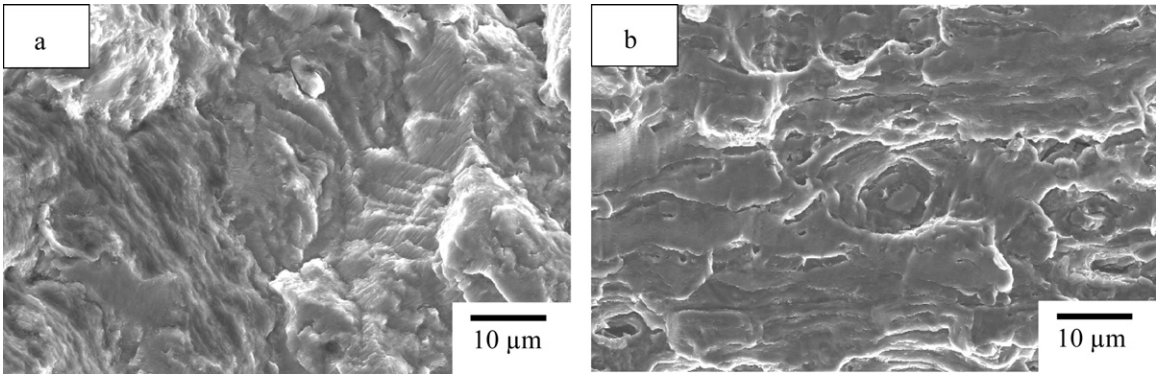

Fig. 10. SEM micrographics showing the fracture surface of (a) 5083, and (b) 5083-FSP.

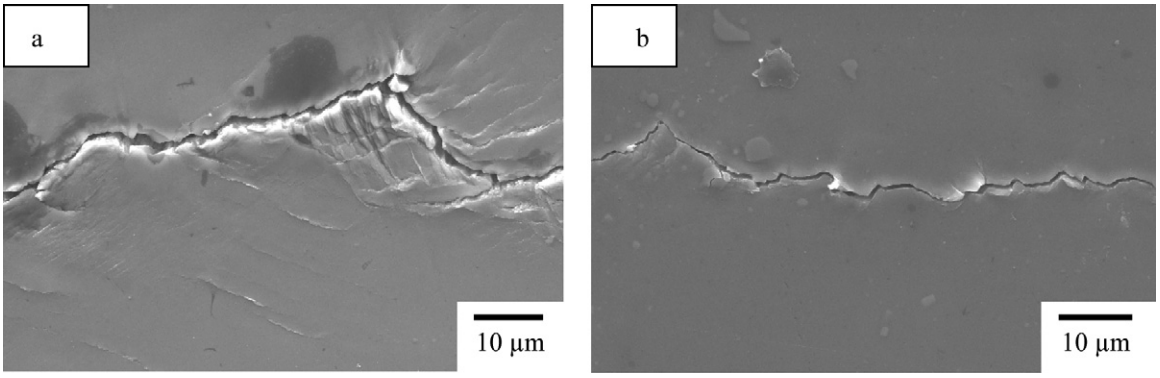

Fig. 11. SEM micrographs showing the crack propagation behavior of (a) 5083, and (b) 5083-FSP (at maximum deflection).

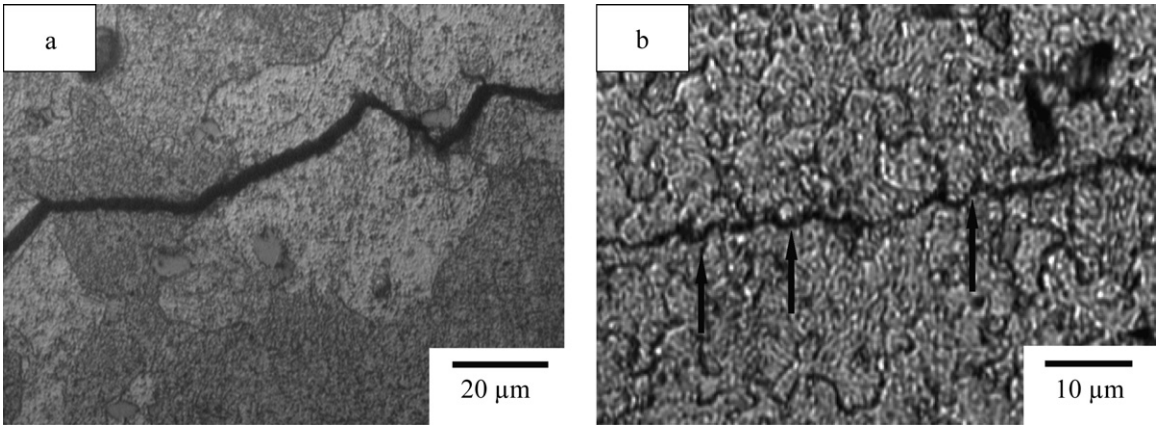

Fig. 12. Optical microstructure of (a) 5083, and (b) 5083-FSP.

Meanwhile, when the deflection amplitude of the 5083-FSP specimen reached the maximum, no slip band appeared in the vicinity of the main crack. This is probably related to the formation of fine grains through dynamic recrystallization in the vicinity of the stir zone. In addition, from observation of the main cracks on the etching specimens of the 5083-FSP and 5083 samples, few differences were found as illustrated in Fig. 12. The crack propagation path of the 5083-FSP specimen is straighter, actually passing through the grain boundary in some places, as shown by an arrow, and this is probably one of reasons why the vibration fracture resistance of the 5083-FSP sample was reduced. The microstructural feature in the vicinity of the notches region can be then elucidated. Consequently, as shown in Figs. 12 and 9, the cracking features of the vibration specimens are related to the crack propagation behavior and their vibration fracture resistance.

4. Discussion

It has been confirmed that the effects of microstructural evolution on tensile properties and vibration fracture resistance of friction stirred Al–Mg alloy are related to the microstructural feature [8]. In addition, referring to FSW process, previous reports also suggest that those fine equiaxed grains at the stir zone are a consequence of dynamic recrystallization during the stirring process

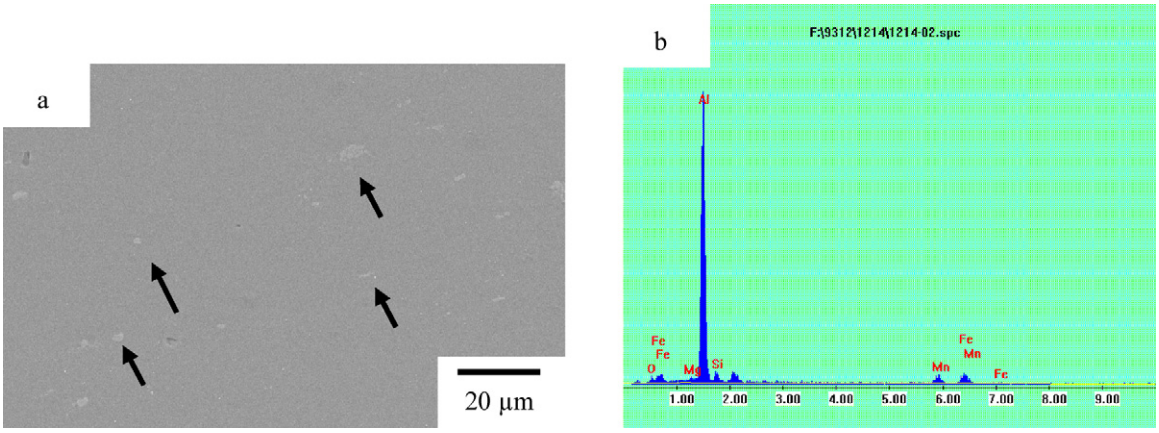

Fig. 13. The distribution of constituent particles mainly consists of Al, Mn, Fe in 5083-FSP sample (a) a SEM image, and (b) the chemical composition analysis (EDS).

of the material. In general, after grain nucleation, there is a possibility that the dynamically recrystallized grains will experience grain growth as the stirring operation continues [9–11]. According to a previous report mentioned above [12], the effect of grain size on the tensile properties of annealed Al–Mg alloy is that the proof stress tends to increase as the grain size decreases, and so does the uniform elongation. Although refining the average grain size can actually improve the proof stress, slight variations in uniform elongation can still be recognized. Nevertheless, from Fig. 8, it should be noted that the effect of average grain size on the uniform elongation of the friction stirred sample does not follow the abovementioned tendency though the average grain size was significantly refined by friction stirring. It is reasonable to suggest that the slight improvement of uniform elongation is affected not only by grain size, but also by other microstructural characteristics such as textural differences and fine particles resulting from high temperature deformation and dynamic recrystallization. The effect of microstructural characteristics should be further examined.

The D–N curves (deflection amplitude vs. numbers of vibration cycles) of the samples could be divided into three stages. In stage I, the initial deflection amplitude is inversely proportional to the damping capacity and the deflection amplitude slightly increases with an increasing vibration cyclic number. According to our microhardness test data on the 5083 alloy, this stage of ascending deflection is associated with increasing work hardening. This increase of work hardening can raise the effective elastic modulus, which can than increase the deflection by reducing the damping capacity. After Stage I, the deflection amplitude increases with a greater vibration cyclic number but not significantly. This duration is designated as stage II and it may result from a lower damping capacity due to strain hardening. As the vibration proceeds, stage III with a drastically decreasing deflection begins. The descending deflection in stage III is due to the deviation of the actual vibration frequency from the resonant frequency caused by the inward propagation of major cracks [13].

Fig. 9(b) shows that both D–N curves have a similar vibration cyclic number when the specimens are tested under constant initial deflection amplitude. Our previous study indicated [12] that the friction stirred Al–Mg alloys had the fine equiaxed recrystallized grains and lower deflection slope (a lower n value) which could reduced the driving force of crack propagation. Consequently, the refining of dynamically recrystallized grain size is advantageous to the vibration life. This result (Fig. 9(b)) suggests that other microstructural factors, in addition to grain size, affect the vibration fracture resistance. To examine the other microstructural factors, details of the microstructure were observed by TEM and SEM. The particles in the 5083-FSP sample were finer than those in the 5083 sample, which resulted from high temperature deformation during FSP as shown in Fig. 6(a) and (b). Sato et al. [14] showed that many Al_6 (Mn, Fe)-type particles were homogeneously distributed in the Friction Stir weld of 5083 alloy. The distribution of the Al_6 (Mn, Fe)-type particles is similar to that of fine particles observed in the present as-received 5083 alloy. Moreover, larger intermetallic particles [such as Al_6 (Mn, Fe) get fragmented to smaller particles due to severe plastic deformation during FSP [15]. A previous study [14] has also shown that the solvus temperature of the Al_6 (Mn, Fe) is higher than the solidus temperature of 5083 Al–Mg alloy. This suggests that Al_6 (Mn, Fe) is not dissolved but stirred with the softened matrix during FSW because FSW is a solid-phase process. Therefore, these particles probably remain in the stir zone of the friction stir welded 5083 Al–Mg alloy, although they can not be clearly observed in TEM images of the stir zones (Fig. 6) due to the very fine grain size. Since Al_6 (Mn, Fe) particles are incoherent to the matrix, they derive the strength of Al alloy through Orowan hardening [16]. In addition, during an analysis of friction stir welds in 5083-O, Svensson et al. [17] found significant variations in the number density of particles between the nugget and the base material. It was found that the density of large (1–10 μm) Mg–Si–O particles reduced in the nugget compared to the base material, and although this was compensated somewhat by an increase in small (0.1–1 μm) particles, it is possible that some dissolution occurred. Fig. 13 also shows that the distribution of large particles mainly consists of Al, Mn and Fe. The EDS analyses of several large particles in all the regions showed most particles to have roughly the same compositions as those particles shown in Fig. 13. Several studies [18,19] have detected many Al_6Mn-type particles in Al alloy 5083, which suggests that the particles in the weld are Al_6 (Mn, Fe). In this study, the Al_6 (Mn, Fe)-type particles were also significantly distributed in the 5083-FSP sample.

In addition, previous study pointed out [14] that the particle distribution could influence the hardness. The Orowan mechanism indicated that the effect of small particles on hardness was roughly uniform throughout the weld. It suggests that the hardness profile mainly depend on the particle distribution in the friction-stir-weld Al alloy containing many small particles. Gliding of mobile dislocations alters from shearing of precipitates to Orowan looping if the precipitates are incoherent. [13] Hence as observed in this study, slip band cracking does not appear in the resonant vibration of the 5083-FSP specimen (Fig. 11(b)). In the stir zone of the 5083-FSP sample, the fine particles act as obstacles to the dislocation movement. This situation suggests that fine particles work more dominantly as obstacles than the grain boundaries because the particles pin the mobile dislocations at smaller intervals than the grain boundaries. This can be correlated with parts of inter-

Table 3
Crack path tortuosity of the 5083 alloy.

Specimen	5083-FSP	5083
Crack path tortuosity	1.08	1.12

granular cracks path shown in Fig. 12(b). As a result, a significant difference in vibration fracture path is recognized in Table 3, which is correlated with the variation in crack tortuosity. In this study, the distribution of finer particles within the dynamic recrystallization grains plays more important role in affecting the vibration fracture resistance. It would be possible to argue that the distribution of the small particles in the stir zone is the main reason why the vibration fracture resistance of the 5083-FSP samples is not significant improved.

5. Conclusion

According to the experimental results discussed in the previous sections, the following conclusions can be drawn:

1. Owing to the increase of work hardening, the deflection increases with increasing number of vibration cycles in the initial stage, which is related to the *n* value. In the final stage, the crack length is sufficiently large and hence the vibration is no longer resonant. Crack propagation in this stage causes the deflection to decrease with increasing number of vibration cycles.
2. As compared with the parent plate, after FSP, the microstructures of specimens achieve grain refinement. The tensile deformation resistance and uniform elongation will increase after the FSP is performed. In particular, the yield stress can be significantly improved after the microstructure is refined during dynamic recrystallization.
3. The vibration life can be defined as the number of critical vibration cycles when the deflection amplitude drops from the maximum deflection. The D–N curve shows the vibration fracture resistance of the friction stirred sample is only slightly better than that of base metal.
4. Judging from the microstructural feature, it can be concluded that the crack propagation resistance is not only grain size dependent but also fine particle dependent.

Acknowledgement

Financial support from the National Science Council of Taiwan is gratefully acknowledged (contract no. NSC 96-2221-E-006-104).

References

[1] D.S. Jiang, T.S. Lui, L.H. Chen, Scripta Mater. 36 (1997) 15–20.
[2] J.Q. Su, T.W. Nelson, R. Mishra, M. Mahoney, Acta Mater. 51 (2003) 713–729.
[3] R.W. Davies, G.J. Grant, H. Eddie Oliver, M.A. Khaleel, M.T. Smith, Metall. Mater. Trans. A 32 (2001) 275.
[4] R.S. Mishra, M.W. Mahoney, S.X. McFadden, N.A. Mara, A.K. Mukherjee, Scripta Mater. 42 (2000) 163.
[5] I. Charit, R.S. Mishra, J. Mater. Res. 19 (2004) 3329–3342.
[6] M. Bournane, M. Nedjar, A.F. Sirenko, Scripta Mater. 40 (1999) 375–382.
[7] G.W.J. Waldron, Acta Metall. 13 (1965) 897–906.
[8] K.T. Huang, T.S. Lui, L.H. Chen, Mater. Trans. JIM 45 (2004) 3216–3222.
[9] K.V. Jata, S.L. Semiatin, Scripta Mater. 43 (2000) 743–749.
[10] O.V. Flores, C. Kennedy, L.E. Murr, D. Brown, S. Pappu, B.M. Nowak, J.C. McClure, Scripta Mater. 38 (1998) 703–708.
[11] L.E. Murr, G. Liu, J.C. McClure, J. Mater. Sci. Lett. 16 (1997) 1801–1803.
[12] K.T. Huang, T.S. Lui, L.H. Chen, Mater. Trans. JIM 47 (2006) 2405–2412.
[13] D.S. Jiang, T.S. Lui, L.H. Chen, Mater. Trans. JIM 41 (2000) 499–506.
[14] Y.S. Sato, S.H.C. Park, H. Kokawa, Metall. Mater. Trans. A 32 (2001) 3033.
[15] M. Karlsen, O. Frigaard, H. Hjelen, O. Grong, H. Norum, Mater. Sci. Forum (2003) 426–432.
[16] J. D. Verhoeven, Fundamentals of Physical Metallurgy, Wiley, New York, p. 118, 1975.
[17] L.E. Svensson, L. Karlsson, L.H. Larsson, B. Karlsson, M. Karlsson, J. Sci. Technol. Weld 5 (2000) 285–296.
[18] K. Kannan, C.H. Johnmson, C.H. Hamilton, Metall. Mater. Trans. A 29A (1998) 1211–1220.
[19] H.B. Mcshane, C.P. Lee, T. Sheppard, Mater. Sci. Technol. 6 (1990) 428–440.